Fuel 303 (2021) 121218

Contents lists available at ScienceDirect

Fuel

journal homepage: www.elsevier.com/locate/fuel

Full Length Article

Modification of the Wiebe function for methane-air and oxy-methane-based spark-ignition engines

Shah Saud Alam [a,*], Scott Wilson Rosa [b], Christopher Depcik [a], Sindhu Preetham Burugupally [c], Ethan McDaniel [c], Jared D. Hobeck [d]

[a] Department of Mechanical Engineering, University of Kansas, Lawrence, KS 66045-7609, United States
[b] Department of Aerospace Engineering, University of Kansas, Lawrence, KS 66045-7609, United States
[c] Department of Mechanical Engineering, Wichita State University, Wichita, KS 67260, United States
[d] Alan Levin Department of Mechanical and Nuclear Engineering, Kansas State University, Manhattan, KS 66506, United States

ARTICLE INFO

Keywords:
Adaptive Wiebe model
Methane combustion
Oxy-methane
Spark-ignition
Combustion duration
Burn rate

ABSTRACT

Predictive combustion models assess engine performance for given setpoints by determining the rate of heat release that is governed by the fuel mass burned. Often, simple mathematical functions such as the Wiebe function are used in simulations to provide mass fraction burned values at each integrated step. Despite its popularity, a limitation of the Wiebe function is that it generally does not take operating conditions into account. Therefore, there is a need for an adaptive Wiebe function that can be scaled for a given fuel and run-time conditions. Here, this is accomplished for methane-air combustion in a spark-ignition (SI) engine. A linear regression analysis was used to fit the adaptive Wiebe model to experimental data with an average R^2 value of 0.965. The scaling process was expanded to include oxy-methane combustion for specialized SI applications, e.g., for stationary or mobile power generation in environments such as Mars. This was accomplished through an analysis of the laminar and turbulent flame speeds that dominate the combustion process and the charge burnup time. The results show that a relative increase in the turbulent flame speeds during oxy-methane combustion shrinks the combustion duration between 10% and 90% mass fraction burned by approximately 87% relative to air. Comparing these results with literature reveals that the scaled Wiebe function follows theory closely and is a reasonable tool for burnt mass and combustion duration predictions.

1. Introduction

Combustion modeling plays an important role in the assessment of internal combustion engine (ICE) performance via prediction of the in-cylinder pressure as a function of the crank angle (or time). In this regard, literature shows that combustion models for Spark Ignition (SI) engines often employ continuous mathematical functions to provide a respectively fast and cost-effective means to predict the burnt fuel mass fraction. One of the most popular tools is the Wiebe function that was proposed by Ivan Wiebe in the 1950's [1]. Originally proposed for use in SI ICEs, modified forms of the function exist, ranging from single-Wiebe to multiple-Wiebe functions for both SI and compression-ignition engine models.

The classical form of the Wiebe function is given in Eq. (1). While originally the Wiebe function predicted the mass fraction burned (Y_b) as a function of crank angle (θ), it may be converted to the time domain upon the inclusion of reaction kinetics [2–4]. Alternatively, the first derivative of the Wiebe function can be used by coupling the resulting expression (Eq. (2)) with the combustion model's system of ordinary differential equations to predict the rate of fuel burned per crank angle (or time), i.e., burn rate [5,6]:

$$Y_b = 1 - exp\left[- a_w \cdot \left(\frac{\theta - \theta_{ign}}{\Delta\theta_d} \right)^{m_w+1} \right] \tag{1}$$

$$\frac{dY_b}{d\theta} = a_w \cdot \frac{(m_w + 1)}{\Delta\theta_d} \cdot \left(\frac{\theta - \theta_{ign}}{\Delta\theta_d} \right)^{m_w} \cdot exp\left[- a_w \cdot \left(\frac{\theta - \theta_{ign}}{\Delta\theta_d} \right)^{m_w+1} \right] \tag{2}$$

where the parameters a_w, m_w, θ_{ign}, and $\Delta\theta_d$ depend on fuel properties and operational conditions [5]. The frequently used values of a_w and m_w for petroleum gasoline are 5 and 2, respectively [5,7–14].

* Corresponding author.
E-mail addresses: ssalam@ku.edu (S.S. Alam), scottrosa@ku.edu (S.W. Rosa), depcik@ku.edu (C. Depcik), sindhupreetham.burugupally@wichita.edu (S. Preetham Burugupally), eemcdaniel@shockers.wichita.edu (E. McDaniel), jdhobeck@ksu.edu (J.D. Hobeck).

https://doi.org/10.1016/j.fuel.2021.121218
Received 18 March 2021; Received in revised form 3 June 2021; Accepted 5 June 2021
Available online 3 July 2021

Nomenclature

Wiebe-specific

a_w	Extent of complete combustion (-)
$\Delta\theta_d$	Combustion duration (°)
$\Delta\theta_{d,new}$	New combustion duration for oxy-methane combustion (°)
$\Delta\theta_{0\text{-}90\%}$	Combustion duration between 0 and 90% mass fraction burned (°)
Δt_d	Combustion duration (s)
$dY_b/d\theta$	Rate of mass fraction burned (1/°)
m_w	Burn rate (-)
θ	Instantaneous step (°)
t	Instantaneous step (s)
θ_{ign}	Ignition crank angle (°)
t_{ign}	Ignition timing (s)
t_{spk}	Spark timing (s)
Y_b	Mass fraction burned (-)

Other Variables and Symbols:

$A - Q$	Wiebe parameter estimation coefficients (-)
A_e	Entrained surface area (m^2)
α	Temperature exponent (-)
β	Pressure exponent (-)
λ	Taylor microscale (m)
m_b	Mass burned (kg)
m_e	Mass entrained (kg)
ϕ	Equivalence ratio (-)
p_{in}	Intake manifold pressure (Pa)
p_{ref}	Reference pressure (Pa)
p_u	Unburned pressure of mixture not yet entrained by flame front (Pa)
r_c	Compression ratio (-)
ρ_u	Unburned charge density of mixture not yet entrained by flame front (kg/m^3)
S_0	Laminar flame speed at atmospheric conditions (m/s or cm/s)
S_L	Laminar flame speed (m/s or cm/s)
S_T	Turbulent flame speed (m/s or cm/s)
τ	Time for combustion (s)
τ_b	Burnup time (s)
θ_{spk}	Spark timing (°)
T_{ref}	Reference temperature (K)
T_u	Unburned temperature of mixture not yet entrained by flame front (K)
U_p	Mean piston speed (m/s)
u'	Turbulent intensity (m/s)
U_{ref}	Reference piston speed (m/s)
X	Scaling factor (-)
Z	Estimation factor (-)

Abbreviations

CI	Compression Ignition
CNG	Compressed Natural Gas
EGR	Exhaust Gas Recirculation
HCCI	Homogeneous Charge Compression Ignition
ICE	Internal Combustion Engine
LTC	Low-Temperature Combustion
MFB	Mass Fraction Burned
NG	Natural Gas
PFI	Port-Fuel Injection (Injected)
ROHR	Rate of Heat Release (J/°)
RON	Research Octane Number
SI	Spark Ignition
TDC	Top Dead Center

Chemical Formulas

C_2H_6	Ethane
CH_4	Methane
H_2	Hydrogen

Subscripts

b	Burned
d	Duration
ign	Ignition
in	Intake
spk	Spark timing
w	Wiebe

A review of the literature finds that default values for a_w and m_w are often adopted directly in combustion models irrespective of the type of fuel, operating conditions (such as intake pressure, equivalence ratio, spark timing, etc.), and the type of oxidizer. Ideally, Wiebe parameters must change with fuel characteristics (due to differing combustion results) and run-time conditions (due to their influence on the burn rates). While the default Wiebe parameter values may provide a decent starting point for a combustion model, they should be updated for specific scenarios to maintain reliability.

To illustrate how the Wiebe parameters were updated for specific situations, methane (alternatively, natural gas) fueled SI engines are considered in this effort. Methane as a fuel has gained traction over the last few decades due to its reduced carbon dioxide emissions [15]. Furthermore, the use of methane in dual-fuel engine operation has become more prevalent since it is relatively easy to inject gaseous fuel into the engine via the intake port [16]. Therefore, a significant amount of data exists in the literature for experimental methane combustion in SI engines. On the modeling front, this has encouraged researchers to fit the classical Wiebe function to experimental data.

While methane-fueled SI engines often operate with air as the oxidizer, their applications can also include alternative oxidative environments. For example, the recent success of several back-to-back Mars missions has led to a surge in the research of *in-situ* production of liquid methane and liquid oxygen from atmospheric carbon dioxide and soil moisture, respectively, on Mars for rocket propulsion [17,18]. A successful deployment of this framework could promote the use of methane-fueled SI engines on Mars for stationary and mobile applications [19,20]. It is important to note that other power generation options for Mars are possible. For instance, nuclear is a potential choice [21,22]. However, since most nuclear power options for other worlds are based on heat produced through radioisotope decay [23,24], the energy density is respectively low for ground and air operations. Fuel cells can provide this needed power [25,26]. Unfortunately, as discussed by Vilekar et al. [27], a proton exchange membrane fuel cell operating on methane would require a complicated reforming and carbon monoxide removal system; whereas, methane-fueled solid oxide fuel cells or solid oxide electrolysis cells have issues with carbon deposits and/or poor activity while also requiring operation at relatively high temperatures (700–800 °C). An effort by Depcik et al. [28] that compared lithium-ion batteries, fuel cells, and combustion engines for a hydrogen-powered unmanned aerial vehicle sheds further insight. Overall, it was found that an internal combustion engine has the greatest potential for mobility with fuel cells having a lower power density. Thus, these findings fall in line with others who indicate the potential use of combustion engines for power on Mars [29–31]. Due to scarcity of atmospheric oxygen on Mars, pressurized oxygen would be required to assist

fuel combustion for stable engine operation. Therefore, it is important to update the Wiebe model for oxygen-assisted combustion. In this regard, this paper presents a framework to scale the Wiebe function for scenarios ranging from air-abundant to air-less operation while also factoring in the effect of engine runtime conditions on combustion characteristics.

Initially, a literature review sheds light on Wiebe function variants for methane combustion in air. Then, an adaptive Wiebe function is presented to include the influence of operational conditions on Wiebe parameters. This model adapts its coefficients by fitting the model to methane-air mass fraction burned (MFB) data available from the literature. Since no such data exists for oxy-methane combustion, a scaling approach is introduced that is based on laminar and turbulent flame speeds in pure oxygen-based combustion environments. The results show that the method devised to update the Wiebe parameters based on dominant factors is deployable under varying operating conditions.

1.1. Review of methane-based versions

Before investigating Wiebe functions for methane combustion, it is important to take note of some of its properties that make it advantageous as an SI engine fuel. Methane is the simplest alkane-based hydrocarbon fuel with a high-octane number (RON > 120) that allows for significantly high compression ratios resulting in enhanced efficiencies as compared to turbocharged gasoline engines. In addition, methane's flexibility as a fuel for lean-burn applications and its lowered emissions during cold-start as well as low-temperature combustion (LTC) are also advantageous [32]. Therefore, methane has become a popular gaseous fuel for SI engine application that is delivered via either port-fuel injection (PFI) or direct-injection [33]. To maintain cost-effective production, methane is often supplied as the primary constituent (≈ 75 – 98 vol%) in a homogeneous mixture of gases [34]. Based on the feedstock used for methane production, this mixture of gases may be indicated as natural gas, compressed natural gas, or biogas. Often, the composition of these mixtures varies based on its place and time of origin as well as the treatment processes used during its production.

Methane does have some disadvantages as a transportation fuel. Firstly, methane is packaged in pressurized tanks that are heavy and pose as range limiters (for transport applications). Furthermore, methane gas injection via the intake port displaces the oxidizer that supports combustion and, therefore, results in reduced volumetric efficiency of the engine. Consequently, methane combustion generally has a relatively lower heat release as compared to gasoline-air mixtures at similar equivalence ratios [32]. These reductions are often overcome by improving the combustion chamber design for increased turbulence, or by varying the initial conditions, such as the injection pressure, injection timing, injection duration, and spark timing [15,32]. Since validating these strategies would otherwise require extensive experimentation, combustion models are often used to examine engine performance over a range of initial setpoints. A review of available Wiebe functions for methane-based operations and their parameters presented in Table 1 reflect the impact of employing these strategies by lumping combustion effects into values of a_w, m_w, and $\Delta\theta_d$.

Of note, due to their relatively significant methane content, Table 1 also lists Wiebe parameters for natural-gas, biogas, or compressed natural gas driven engines to understand the potential range of Wiebe parameters. It is evident from Table 1 that fuel composition and combustion strategies can affect the choice of Wiebe parameters. While some researchers prefer to use standard values for these variables, others work with differing degrees of freedom by setting some parameters constant while changing others to fit data. Overall, these values should not be readily imported into a combustion model without considering

Table 1
Existing Wiebe models and their corresponding a_w, m_w, and $\Delta\theta_d$ values in literature with fuel compositions (major species only for brevity) listed.

a_w	m_w	$\Delta\theta_d$ or time (*degree* or ms)	Wiebe Model Used	Fuel with % composition	Reference
2.8	2.4	Depends primarily on ϕ	$Y_b = 1 - exp\left[-a_w \cdot \left(\frac{\theta-\theta_{ign}}{\Delta\theta_d}\right)^{m_w+1}\right]$	CH_4: 80% H_2: 20%	[35,36]
4.9	2.0	≈ 51°	$Y_b = 1 - exp\left[-a_w \cdot \left(\frac{\theta-\theta_{ign}}{\Delta\theta_d}\right)^{m_w+1}\right]$	CNG ($CH_4 \geq$ 90%)	[37]
5	2	(1 ms)	$Y_b = 1 - exp\left[-a_w \cdot \left(\frac{t-t_{ign}}{\Delta t_d}\right)^{m_w+1}\right]$	CH_4: 90%	[2]
5	2	(2.25 ms)	$Y_b = 1 - exp\left[-a_w \cdot \left(\frac{t-t_{spk}}{\Delta t_d}\right)^{m_w+1}\right]$	NG (CH_4: 86%, C_2H_6: 12%)	[3]
5	2	(1 ms)	$Y_b = 1 - exp\left[-a_w \cdot \left(\frac{t-t_{ign}}{\Delta t_d}\right)^{m_w+1}\right]$	CH_4: 100%	[4]
5	2	37° – 41°	$Y_b = 1 - exp\left[-a_w \cdot \left(\frac{\theta-\theta_{ign}}{\Delta\theta_d}\right)^{m_w+1}\right]$	CH_4: 92.285% C_2H_6: 5.455%	[38]
5	2	30°	$Y_b = 1 - exp\left[-a_w \cdot \left(\frac{\theta-\theta_{spk}}{\Delta\theta_d}\right)^{m_w+1}\right]$	CH_4: 100%	[39]
5	2.2	N/A	$Y_b = 1 - exp\left[-a_w \cdot \left(\frac{\Delta\theta}{\Delta\theta_d}\right)^{m_w+1}\right]$	CH_4: 100%	[40]
7.04 – 10.18	3.5 – 4.4	58° – 98.4°	$Y_b = 1 - exp\left[-a_w \cdot \left(\frac{\Delta\theta}{\Delta\theta_d}\right)^{m_w+1}\right]$	NG (CH_4: 98.5%)	[41]
7.78 – 10.36	0.96 – 1.13	58° – 67°	$Y_b = 1 - exp\left[-a_w \cdot \left(\frac{\theta-\theta_{ign}}{\Delta\theta_d}\right)^{m_w+1}\right]$	CH_4: 100%	[42]
5	2	N/A	$\frac{dY_b}{d\theta} = \frac{\theta}{\Delta\theta_d} \cdot (m_w+1) \cdot y^{m_w} \cdot exp\left[-a_w \cdot y^{(m_w-1)}\right]$	CH_4: 100%	[6]
5	1.42	≈ 40°	$Y_b = 1 - exp\left[-a_w \cdot \left(\frac{\theta-\theta_{ign}}{\Delta\theta_d}\right)^{m_w+1}\right]$	CH_4: 100%	[43]
5.64	2.73	50°	$Y_b = 1 - exp\left[-a_w \cdot \left(\frac{\theta-\theta_{ign}}{\Delta\theta_d}\right)^{m_w+1}\right]$	CH_4: 99.5%	[44]
4	2	N/A	$Y_b = 1 - exp\left[-a_w \cdot \left(\frac{\theta-\theta_{ign}}{\Delta\theta_d}\right)^{m_w+1}\right]$	$CH_4 \geq$ 99%	[45]
N/A	3	N/A	$Y_b = 1 - exp\left[-a_w \cdot \left(\frac{\theta-\theta_{ign}}{\Delta\theta_d}\right)^{m_w+1}\right]$	CH_4: 100%	[46]
2.815	0	25.4°	$Y_b = 1 - exp\left[-a_w \cdot \left(\frac{\theta-\theta_{ign}}{\Delta\theta_d}\right)^{m_w+1}\right]$	NG (CH_4: 96.023%, C_2H_6: 2.036%)	[47]
2.303	N/A	N/A	$Y_b = 1 - exp\left[-a_w \cdot \left(\frac{\theta-\theta_{ign}}{\Delta\theta_{0-90\%}}\right)^{m_w+1}\right]$	NG (CH_4: 94.99%, C_2H_6: 2.50%)	[48]

the effect of specific operating conditions and engine geometry (e.g., compression ratio). In this regard, the adaptive Wiebe model proposed by Alam and Depcik [49] that bases Wiebe parameters (a_w, m_w, and $\Delta\theta_d$) for a hydrogen-fueled PFI SI engine on geometric and operational values provides a means to estimate pertinent parameters. This model is updated in this effort through its application to methane and then extended to account for oxy-methane combustion. Of importance regarding available methane data used for calibration (indicated in Section 1.3), only data for four-stroke ICEs and higher CH_4 concentrations (>90%) were used for consistency.

1.2. Adaptive Wiebe model

The adaptive Wiebe model computes the parameters of the classical Wiebe function while considering their interdependency on pertinent engine geometric parameters and run-time conditions as shown in Eqs. (3)-(6). Of note, these equations were updated from the former effort by normalizing some of the parameters with a reference pressure ($p_{ref} = 1$ bar) and reference mean piston speed ($U_{ref} = 1$ m/s) to keep the Wiebe parameters dimensionless. Moreover, exhaust gas recirculation (EGR) terms in the prior effort (introduced in Section 1.1) were omitted since no MFB data including the influence of EGR was found for a methane-operated engine. Overall, the coefficients A through Q (excluding K) are computed by fitting the Wiebe model to data extrapolated from peer-reviewed literature (shown in Section 1.3).

$$a_w = A + B\cdot r_c + C\cdot\frac{p_{in}}{p_{ref}} - D\cdot\frac{U_p}{U_{ref}} + E\cdot\phi \tag{3}$$

$$m_w = F - G\cdot r_c - H\cdot\frac{p_{in}}{p_{ref}} + I\cdot\frac{U_p}{U_{ref}} - J\cdot\phi \tag{4}$$

$$\Delta\theta_d = K - L\cdot r_c - M\cdot\frac{p_{in}}{p_{ref}} + N\cdot\frac{U_p}{U_{ref}} - O\cdot\phi \tag{5}$$

$$K = P + Q\left|\theta_{spk}\right| \tag{6}$$

where r_c is the engine compression ratio, p_{in} is the intake manifold pressure, U_p is the mean piston speed, ϕ is the equivalence ratio, and θ_{spk} is the spark timing.

For brevity, a quick description is provided here and summarized in Table 2 to aid the reader's understanding of these interdependencies as described in Heywood [5]. Since a higher engine compression ratio (r_c) results in a hotter fuel–air unburned mixture (T_u) prior to spark initiation, this causes a faster combustion event with a greater heat release rate. Furthermore, an increasing engine load requires opening the throttle plate of a PFI engine to raise the inlet pressure (p_{in}), which results in a denser fuel–air mixture (ρ_u) with a greater amount of potential energy. Upon ignition, this promotes a faster combustion event and effectively reduces the time required for combustion. In addition, in-cylinder turbulence increases with faster engine speeds that reduces the time for combustion. However, for high-RPM engines, the amount of time is respectively smaller than the residence time of the different reactions that comprise the combustion event. While this phenomenon does not affect the maximum burn rate, combustion duration gets relatively prolonged on a crank angle basis. Here, the time factor is believed to outweigh the turbulence influence as highlighted by others [10,50,51]. From the standpoint of chemistry, the equivalence ratio (ϕ) affects the amount of heat released during combustion. The combustion reaction becomes more exothermic with growing equivalence ratios that results in a greater heat release; thus, promoting faster combustion. Finally, moving spark timing (θ_{spk}) closer to top dead center (TDC) results in a hotter burn (since the fuel–air charge is hotter) and leaves relatively warmer end gases that increase the initial temperatures of the subsequent cycle; thus, progressively shortening combustion duration.

Table 2
Interdependent relationships between the Wiebe parameters and engine geometry as well as operating conditions. Key: ↑ (increases), ↓ (decreases), → (move towards).

Parameter	Direction	Physical Effect	a_w	m_w	$\Delta\theta_d$
r_c	↑	T_u↑, Heat Release Rate ↑	↑	↓	↓
p_{in}	↑	ρ_u↑, Heat Release Rate ↑	↑	↓	↓
U_p	↑	τ↑ and $\Delta\theta_d$ ↑	↓	↑	↑
ϕ	↑	Heat Release Rate ↑	↑	↓	↓
θ_{spk}	→ TDC	T_u ↑			↓

The current adaptive Wiebe model deviates slightly from the original version proposed by Alam and Depcik [49]. Formerly, the mean piston speed was found to have no impact on the burn rate or m_w. Since hydrogen was used as the prior fuel, the rapid combustion characteristics of hydrogen and its relatively fast flame speed masked the dependence of m_w on the mean piston speed; thus, making it less noticeable. The available methane data suggests that both a_w and m_w might be impacted by the mean piston speed. The respectively sluggish combustion characteristics of methane as compared to hydrogen results in a somewhat slower burn rate and, thus, the dependence of m_w on the mean piston speed becomes more apparent. A respectively slower burn rate results in a growth of incomplete combustion. Olalekan et al. [52] showed that increasing engine speed results in a relatively faster decline in the burn rate compared to the extent of complete combustion. Therefore, m_w is observed to increase with growing mean piston speed (U_p) while a_w decreases simultaneously.

1.3. Model calibration for methane-air combustion and results

Calibration of the adaptive Wiebe model employed experimentally observed MFB data gathered from the literature. Due to methane's popularity as a fuel, there are available data (in the form of figures and illustrations) that the current effort relies upon [37,41,42,44,53–56]. Data capture software, such as WebPlotDigitizer, was used to estimate data from the figures for use in model calibration [57]. Ensuring that all data collected from the literature was applicable to the model was critical for accurate model calibration. For example, the efforts of Babu et al. [53] focused on a prolonged combustion process that required multiple Wiebe functions to predict the MFB; therefore, this data would not be appropriate to use for calibrating a single Wiebe function model such as the current study. Fig. 1 shows the data used for calibration.

After retaining the pertinent data, the adaptive Wiebe model is fit to

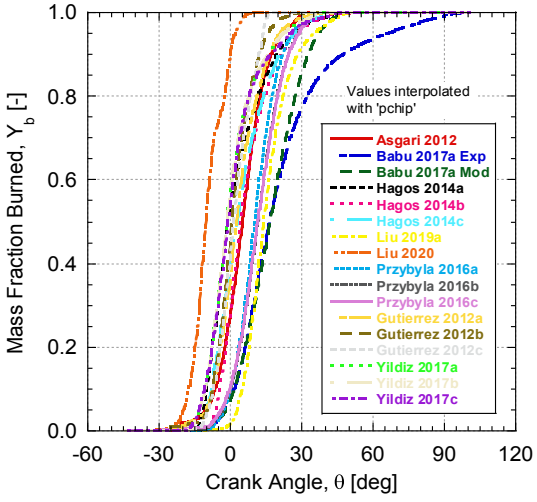

Fig. 1. Experimental MFB data (modified using *piecewise cubic Hermite interpolating polynomial (pchip)*) as a function of crank angle [37,41,42,44,53–56]. Key: Exp (experimental), Mod (model); a, b, and c signify different sets of data from the same paper.

these MFB profiles by adjusting the coefficients *A* through *Q* of Eqs. (3)–(6). Here, a linear regression approach coupled with MATLAB's *fmincon* routine finds the correct coefficients by minimizing the residuals for each dataset over 100,000 simulations. Specifically, the optimization procedure begins by employing a random number generator to set the initial values for every Wiebe parameter. This random number generator eliminates any bias that would otherwise occur. In addition, these initial values are bound by the minimum and maximum values for each Wiebe parameter taken from the sifted data ($1 < a_w < 7$, $0.1 < m_w < 3$, $5^\circ < \Delta\theta_d < 120^\circ$) that further ensures meaningful results. After 100,000 simulations, the resulting coefficients listed in Table 3 converged the residual to the set criteria (1E-5) and increasing the number of simulations did not yield any noticeable changes in the coefficient values. The coefficients produce a mean R^2 value of 0.965 for the data shown in Fig. 1 versus model predictions using Eqs. (3)–(6).

It is worth noting that a greater amount of MFB data for model optimization will influence these coefficients while promoting a wider applicability of the resulting model. Since incorrect data can introduce errors in the model and the subsequent analysis, it is critical to select the correct data for model optimization. Then, the model is validated via parametric study by varying engine geometric and operational parameters, and upon successful validation, the adaptive Wiebe model is used to predict the MFB for the literature data selected for model optimization.

1.3.1. Parametric studies

After computing the Wiebe parameters from the coefficients using Eqs. (3)–(6), the parameters of these equations are varied independently of each other to determine MFB profiles. Fig. 2 shows the resulting MFB profiles that are later compared with the theory presented in Section 1.2 for validation.

Fig. 2a shows the effect of changing the initial compression ratio on the resulting MFB profiles at constant spark timing. Theoretically, the rate of entrainment of the methane-air mixture should grow with increasing compression ratio due to the growing turbulence and smaller eddies. Furthermore, the in-cylinder temperature before combustion rises with compression ratio from the equation of state; thus, in-cylinder conditions prior to combustion would promote a burn faster and a relatively greater rate of heat release. This, in turn, accelerates the overall combustion process by lowering the ignition threshold in subsequent thermodynamic cycles. This phenomenon is accurately reflected in Fig. 2a that shows a faster burn rate and shortened combustion duration at higher compression ratios.

Fig. 2b demonstrates a similar outcome with increasing load (p_{in}). The faster burn rate and shortened combustion duration is based upon the increasing amount of air and fuel mixture inducted with greater load. A denser charge is inducted into the cylinder per thermodynamic cycle with a larger amount of potential energy to be released. The greater rate of heat release from increased charge mass leaves hotter end gas temperatures that shorten the combustion duration in subsequent cycles until a steady state is achieved. Therefore, the model predictions of Fig. 2b correctly align with theory.

Fig. 2c shows the model response for increasing engine speed. Here, since combustion of the inducted charge takes longer on a per crank angle basis at higher engine speeds, the maximum burn rate remains relatively unaffected. The overall combustion duration and profile experiences minimal change with increasing speed, which is accurately predicted by the model. When the equivalence ratio is increased, the 50% MFB point shifts earlier, signifying a faster burn rate and a shorter combustion event as shown in Fig. 2d. This occurs due to the increased exothermicity of the ensuing combustion reaction that results in a relatively larger rate of heat release and higher adiabatic flame temperatures; thus, promoting a faster burn. However, the model does not account for significantly rich mixtures where the MFB should decrease due to the excess fuel acting as a heat sink – an anomaly that was considered but omitted (at this time) to keep the model relatively simple. This issue is less likely to pose a problem for real world applications since natural gas engines usually operate under lean conditions for maximum efficiency [58].

Finally, Fig. 2e shows that moving the spark timing closer to top dead center (TDC) results in an enhanced burn rate and shorter combustion duration. Since the in-cylinder temperature and pressure are greatest near TDC, the ignition threshold of the combustible mixture is lowered. Igniting the charge under these conditions liberates a relatively large amount of chemical energy within a few crank angles. The burn rate becomes steep and combustion duration is reduced. However, moving the spark timing away from TDC slows down the combustion process due to lowered in-cylinder pressures and temperatures prior to ignition – consequently, reducing the burn rate while increasing the overall time for combustion. Overall, the model follows theory and predicts correct trends for varying governing parameters.

Table 3
Coefficients to determine the Wiebe parameters for the adaptive Wiebe model.

Coefficient	Value	Units
A	−8.584E + 00	–
B	4.306E-01	–
C	2.716E + 00	–
D	1.006E-02	–
E	4.348E + 00	–
F	2.029E + 00	–
G	6.200E-04	–
H	5.100E-04	–
I	1.009E-02	–
J	2.062E-02	–
L	1.030E-03	–
M	4.390E-03	–
N	1.037E-02	–
O	1.422E-02	–
P	2.770E + 01	–
Q	6.632E-01	–

1.3.2. Model validation

The validation procedure involves predicting MFB profiles for the cases shown in Fig. 1. For brevity, only a select few are presented with Fig. 3 showing varying levels of confidence in the model predictions for the experimental data of Gutierrez [54], Yildiz et al. [42] and Babu et al. [53]. The main criteria for accuracy come from observing model behavior in three MFB zones, e.g., 0–10%, 10–90%, and 90–100% burn regions. Here, representative high, average, and low accuracy results according to R^2 values are provided to indicate the predictive nature of the model. As mentioned prior, the model's mean R^2 value is 0.965.

It is observed from Fig. 3a that the computed Wiebe parameters accurately predict MFB profiles in all three zones resulting in a relatively higher R^2 value with negligible difference between experimental and model-predicted 50% burn points. Of note, Gutierrez [54] used a modified compression ignition (CI) engine for their natural gas SI combustion experiments. Since the original CI engine had a 41° valve overlap, the valve camshaft was modified to reduce the overlap and minimize its influence on combustion performance. On the other hand, Fig. 3b shows that the predicted 50% burn point deviates significantly from the experimental datapoint, suggesting a slower burn rate (since it deviates to the right). However, both the extent of complete combustion and the combustion duration are similar between the experiment and model. While this results in a relatively high confidence ($R^2 > 0.9$), it is recommended to find and add similar data from other studies to determine the coefficients (as described in Section 1.3). Finally, Fig. 3c shows the least confidence in the model. This is primarily due to two reasons: a) Babu et. al, [53] converted a CI engine into an SI engine without altering the valve lift timing unlike Gutierrez [54], and b) the relative slowdown of the combustion process during the latter crank angles of the expansion stroke; thus, exhibiting a mixing-controlled (diffusion) burn. Since a multiple-Wiebe function predicts this type of event relatively better,

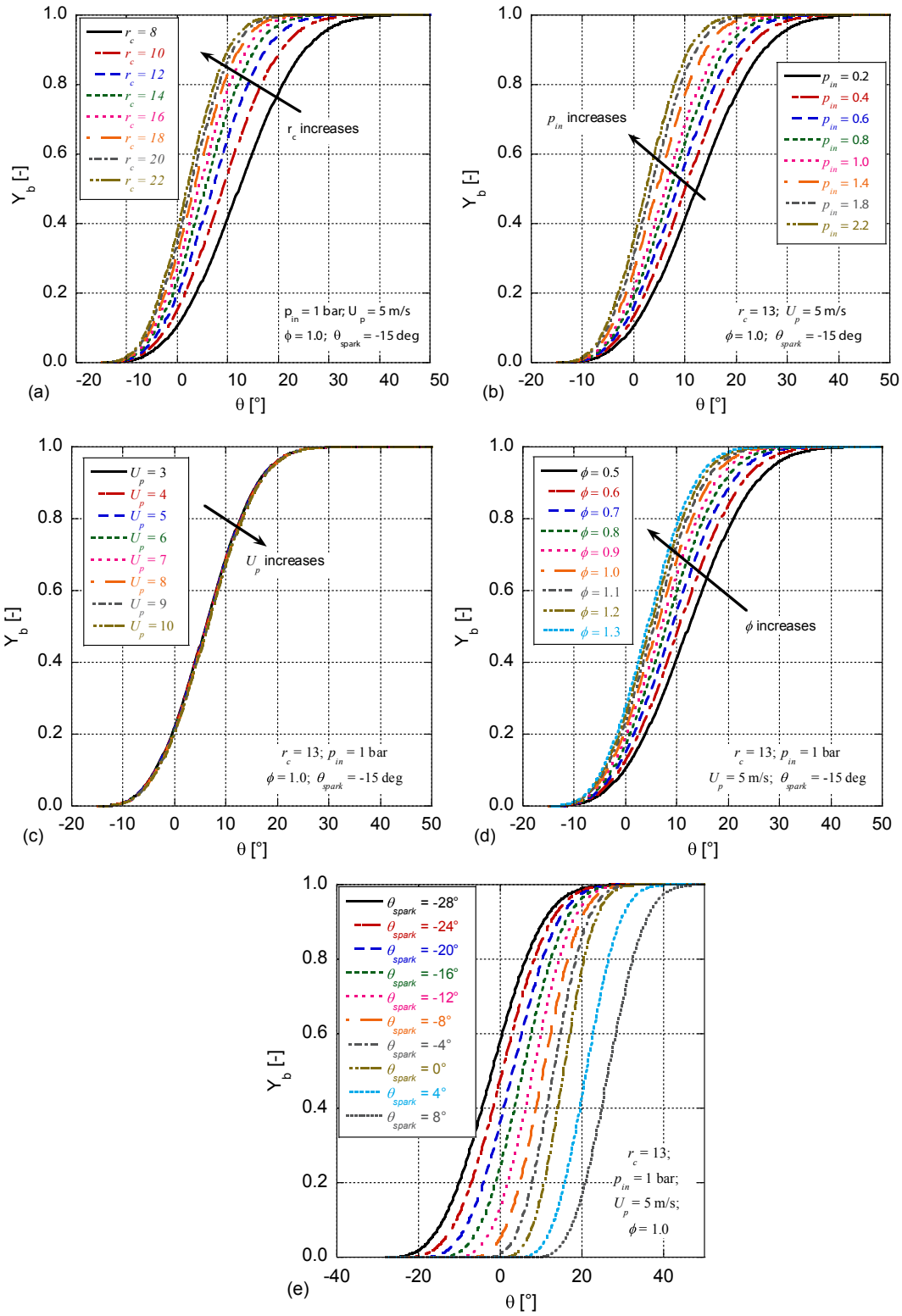

Fig. 2. Parametric study showing the MFB profiles predicted by the adaptive Wiebe model for varying initial conditions.

representing it by a single-Wiebe function gives erroneous results. Consequently, including such data for coefficient determination affects the results and it is advised to treat the model with caution. Ideally, it is safer to neglect them during model calibration.

At this point, while the resulting model for methane-air combustion in SI engines reasonably simulates Earth applications, it will fail when used for specialized engine applications. This includes operation in alien environments like Mars where atmospheric air is not available. In this scenario, the possible use of oxygen tanks can ensure combustion power. The methane-air model must be modified further to consider the change in burn characteristics resulting from oxy-methane combustion.

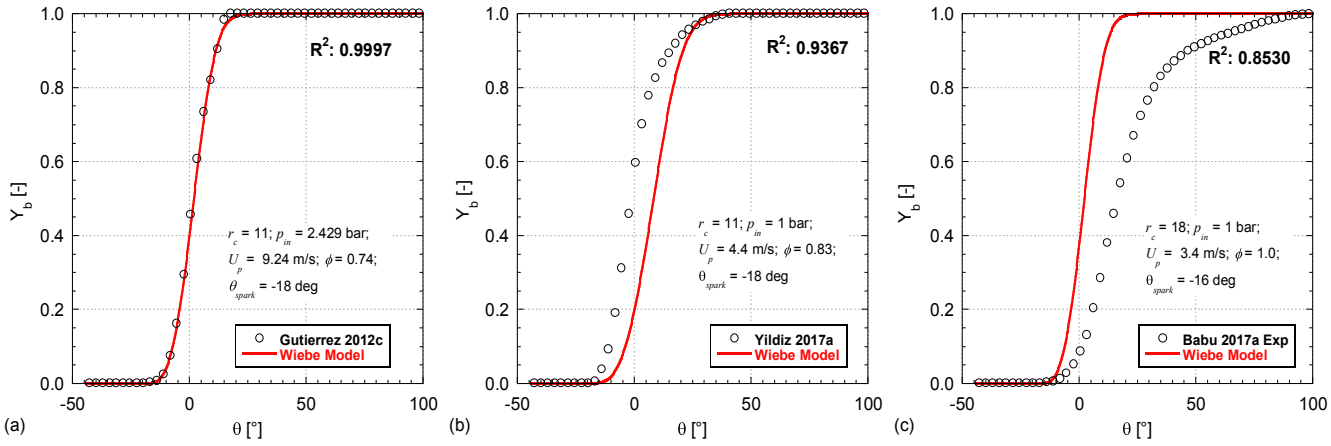

Fig. 3. Cases showing decreasing confidence (left to right) in model results [42,53,54].

2. Oxy-methane combustion

Generally, SI models for ICEs calculate flame propagation and combustion via the rate of mass entrained (m_e) along with the rate at which it burns (m_b) [59–61], respectively:

$$\frac{dm_e}{dt} = \rho_u \cdot A_e \cdot (u' + S_L) \tag{7}$$

$$\frac{dm_b}{dt} = \frac{m_e - m_b}{\tau_b}\ \tau_b = \frac{\lambda}{S_L} \tag{8}$$

where A_e is the entrainment area, u' is the turbulence intensity, S_L is the laminar flame speed, τ_b is the characteristic burning time for the unburned mixture, and λ is the Taylor microscale. Since S_L is the unburned gas velocity in a direction normal to the combustion wave surface [62], it is an important parameter that is used to accurately predict the fuel burning rates and the associated turbulent flame speeds [63].

2.1. Laminar flame speeds

The laminar flame speeds for a specified fuel are usually determined via Schlieren photography during experiments at atmospheric conditions or via extensive combustion modeling using detailed reaction kinetics. At conditions other than atmospheric, the laminar flame speeds are calculated using the following formula:

$$S_L = S_0 \cdot \left(\frac{T_u}{T_{ref}}\right)^{\alpha} \cdot \left(\frac{p_u}{p_{ref}}\right)^{\beta} \tag{9}$$

that is a function of the unburned temperature and pressure (p_u). In this expression, S_0 is the laminar flame speed at atmospheric conditions (T_{ref} and p_{ref}); whereas, α and β are the temperature and pressure exponents, respectively. Here, parameters α and β are determined by fitting Eq. to data. For accurate predictions of the laminar flame speed, the temperature exponent (α) must remain positive while the pressure exponent (β) must stay negative across all equivalence ratios. In this regard, Varghese et al. [64] studied the behavior of α and β for methane-air flame fronts at equivalence ratios ranging from 0.7 to 1.3 and showed that α and β approach their maxima and minima, respectively, at $\phi \approx 1.1$. In addition, they also indicated the influence of the operating pressure and temperature on α and β, respectively. Based on data from literature [64–66], second-order polynomial fits can be generated for both α and β as a function of the operational equivalence ratio, respectively:

$$\alpha_{CH_4\text{ - air}} = 4.03 \cdot \phi^2 - 8.28 \cdot \phi + 6.06 \tag{10}$$

$$\beta_{CH_4\text{ - air}} = -1.57 \cdot \phi^2 + 3.09 \cdot \phi - 1.89 \tag{11}$$

Pizzuti et al. [66] showed that the laminar flame speeds slow down and stabilize beyond an equivalence ratio of 1.3. As a result, the overall profile can be reproduced with a fourth-order polynomial equation for S_0 at equivalence ratios between 0.6 and 1.6:

$$S_{0,CH_4\text{ - air}}\left[\frac{\text{cm}}{\text{s}}\right] = 420.81 \cdot \phi^4 - 1801.00 \cdot \phi^3 + 2670.80 \cdot \phi^2 - 1592.80 \cdot \phi + 338.53 \tag{12}$$

It is important to reiterate that this model is prone to error outside the equivalence ratio bounds of 0.6 and 1.6.

Expanding the scope of the current investigation to include oxy-methane combustion for engine operation in air-deficient environments required the prediction of laminar flame speeds. Therefore, following a similar approach used for the methane-air framework (Eqs. (10)–(12)), a new set of relationships were defined for oxy-methane despite the relatively limited amount of data available in the literature [67–69].

$$\alpha_{CH_4\text{ - }O_2} = 1.66 \cdot \phi^2 - 4.74 \cdot \phi + 7.08 \tag{13}$$

$$\beta_{CH_4\text{ - }O_2} = -0.93 \cdot \phi^2 + 2.00 \cdot \phi - 1.47 \tag{14}$$

$$S_{0,CH_4\text{ - }O_2}\left[\frac{\text{m}}{\text{s}}\right] = 1.08 \cdot \phi^3 - 6.39 \cdot \phi^2 + 9.47 \cdot \phi - 1.24 \tag{15}$$

Theoretically, an abundance of oxygen during combustion raises the adiabatic flame temperature that promotes the overall reaction speed [63]. The experimental data available from literature [67,69–71] confirms this phenomenon and finds that oxy-methane combustion is significantly faster (8–22 ×) than methane-air combustion at all (considered) equivalence ratios. Due to this growth in combustion speed, evaluation of the laminar flame speed along with the turbulent flame speed and turbulence intensity becomes paramount for scaling the Wiebe parameters.

2.2. Turbulent flame speeds

Tabaczynski et al. [59] indicate that under turbulent operating conditions, the flame propagates with a velocity equal to:

$$S_T = u' + S_L \tag{16}$$

which was originally derived by Damköhler [72] to correlate the turbulent flame speed (S_T), turbulence intensity, and laminar flame speed. Both the turbulent flame speed and the turbulence intensity depend on a detailed knowledge of the operating conditions, internal flow field, equivalence ratios, and fuel characteristics that may be

obtained via extensive combustion modeling and experimentation. However, researchers have tried to simplify these relationships and Ratzke et al. [73] provide a consolidated list of the correlations available in literature for methane-air combustion. Most of these correlations depend on flow-specific parameters, such as the Reynolds and Lewis numbers, that are difficult to quantify. Since Ratzke et al. indicate that a pressure-dependency is required for ICE conditions, the correlation by Kobayashi [74] was chosen since it is in "quantitative accordance" with experimental data and is straightforward to compute:

$$\frac{S_T}{S_L} = 2.9 \cdot \left(\frac{u'}{S_L}\right)^{0.38} \cdot \left(\frac{p_u}{p_{ref}}\right)^{0.38} \tag{17}$$

where p_{ref} is 0.1 MPa and u' is calculated in meters per second. Moreover, Ratzke et al. [73] conducted experiments to determine S_T/S_L ratios at varying equivalence ratios that the following curve-fit reproduces with an R^2 value equal to 0.99:

$$S_T = S_L \cdot \left(200.56 - 530.88 \cdot \phi + 545.34 \cdot \phi^2 - 192.73 \cdot \phi^3\right) \tag{18}$$

2.3. Extension of the Wiebe model

The ratio of the turbulent flame speed of oxy-methane to methane-air combustion is assumed here to provide a reasonable measure of the associated increase in turbulence and overall flame speed. To keep the process relatively simple it is estimated that the Wiebe parameter most influenced by a pure oxygen environment is the combustion duration. While all three Wiebe parameters would most likely be affected, there is no quantitative data or qualitative models that can be reviewed to build a more complex model. Therefore, $\Delta\theta_d$ is scaled as:

$$X = \frac{S_{T_{O_2}}}{S_{T_{air}}} \cdot Z \tag{19}$$

$$\Delta\theta_{d,new} = \frac{\Delta\theta_d}{1 + X} \tag{20}$$

where X is the scaling factor and Z is an estimation factor. The estimation factor Z is based upon the efforts of Kang et al. [75] who showed an approximately 25% reduction in the combustion duration of n-heptane fuel with oxygen compared to air in an Homogeneous Charge Compression Ignition (HCCI) engine. Since such reduction might be an overestimation for methane combustion (due to its sluggish combustion characteristics with air), a 10% reduction is estimated as a reasonable approximation for the current effort.

2.4. Results

The resulting Wiebe model for oxy-methane MFB prediction was investigated by comparing the reduced combustion duration (oxygen-assisted combustion) versus air from Fig. 3a and is shown in Fig. 4. Employing the techniques mentioned in Sections 2.1 through 2.3 finds that the transition from air to oxygen as the oxidizer results in an approximately 87% reduction in the combustion duration (10%-90% MFB) of methane while keeping other operational conditions unchanged. Of note, Fig. 4 compares the resulting profile with the original without adjusting the spark timing to achieve peak in-cylinder pressures at prime crank angles.

While the initial impression of the magnitude of reduction seems unrealistic, there are a few studies in the available literature that potentially support this outcome. Specifically, Van-Blarigan et al. [76] compared the combustion performance of methane in oxygen-enriched environments and reported a 46% reduction in combustion duration when the oxygen concentration was increased from 21% (air) to 36.7% with the rest being EGR. Along with the 25% combustion duration reductions discovered by Kang et al. [75] using n-heptane (a liquid fuel often used as a gasoline surrogate [51]) in HCCI operation with oxygen

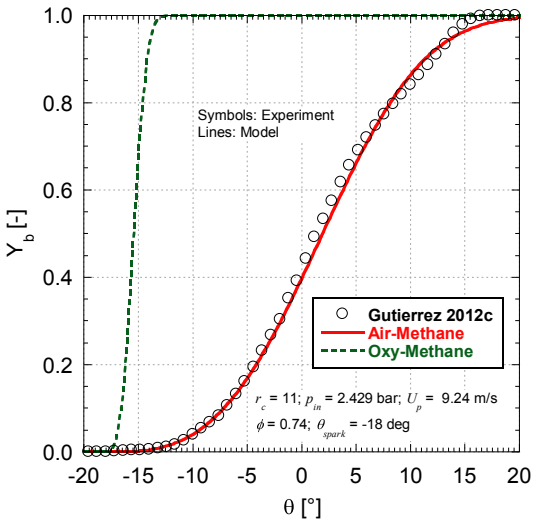

Fig. 4. Combustion duration reductions and burn rate predictions for oxy-methane combustion compared to the methane-air combustion shown in Fig. 3a.

help in concluding that the oxy-methane revision to the adaptive Wiebe model effectively simulates increased mixture homogeneity, greater adiabatic flame temperature, and enhanced laminar and turbulent flame speeds.

3. Discussion

The adaptive Wiebe model appears to be a reasonable tool for the MFB prediction of a given fuel. Initially, basing the model on engine geometry and operational conditions ensures that its behavior is based on theory. Then, modifying the model for air–fuel combustion operation becomes crucial. Since combustion in SI engines occurs in the presence of air, a significant amount of air–fuel combustion data can be used to find the coefficients. The selection of correct data for the model ensures its stability and minimizes the potential for skewed results.

Furthermore, the proposed model offers an adaptability to oxy-fuel combustion by incorporating the ratios of turbulent and laminar flame speeds. Here, the selection of correct data is essential for successful modification. In addition, stabilization of the laminar flame speeds at relatively low or high equivalence ratios governs the polynomial fit. It is important to individually evaluate the behavior of the temperature and pressure exponents, α and β, respectively, of Eq. and validate with theory. Often, the operational temperature and pressure govern these parameters, and thus, the overall laminar flame speed during air–fuel combustion. Finally, the estimation factor, Z, (in Eq. (19)) has a controlling effect on the combustion duration reduction and its value must be selected carefully by reviewing literature, such as that by Kang et al. [75]. Since there is little combustion data available that directly compares pure oxygen environments to the use of air as the oxidizer, no specific methods for determining Z are available in the literature. Thus, this effort provides a first estimate of Z that can be expanded upon by others.

4. Conclusions

For performance assessment under varying conditions, combustion models are preferred over experimental analysis due to time and cost constraints. Since the rate of heat release is governed by the fuel mass burned as a function of the crank angle (or time) in these models, they rely upon popular functions, such as the Wiebe variant, to provide MFB values at each time step. Here, an adaptive Wiebe model was generated to influence the fuel burn rate by engine geometric and operational

conditions. The coefficients used to determine the Wiebe parameters were found by fitting the model to data available from the literature using a linear regression (least-squares) method. This made the adaptive Wiebe model more versatile and setting the upper and lower bounds on the Wiebe parameters and ensured that their values remained accurate. Of note, it is critical to maintain a high average R^2 value to ensure model stability and accuracy – therefore, calibration data must be thoroughly scrutinized prior to analysis.

In addition, the adaptive Wiebe model was modified for a specialized application of fuel combustion in oxygen instead of air. The laminar and turbulent flame speed data were the determining factor in this conversion. This is predominantly due to the comparatively substantial increase in laminar flame speeds in oxy-fuel combustion resulting from significantly higher adiabatic flame temperatures. These faster laminar flame speeds will result in greater turbulence; thus, faster burn rates and shorter combustion durations are expected. This information was factored into the adaptive Wiebe model via the ratio of the turbulent flame speeds encountered during oxy-fuel and air–fuel combustion. For methane combustion, the combustion duration between 10% and 90% MFB is observed to shrink by approximately 87% with the switch from air-assisted to pure-oxygen combustion modes. The efficacy of the results suggests that the scaled adaptive Wiebe model would help in achieving stable engine operation under specialized applications, such as stationary and mobile (transport, aerial, etc.) on Mars.

5. Funding sources

This work was supported by the National Aeronautics and Space Administration [grant number: 80NSSC19M0042].

CRediT authorship contribution statement

Shah Saud Alam: Conceptualization, Data curation, Formal analysis, Investigation, Methodology, Writing - original draft, Software, Validation, Visualization, Writing - review & editing. **Scott Wilson Rosa:** Data curation, Investigation, Software, Writing - review & editing. **Christopher Depcik:** Conceptualization, Data curation, Formal analysis, Funding acquisition, Investigation, Methodology, Project administration, Resources, Software, Supervision, Validation, Visualization, Writing - review & editing. **Sindhu Preetham Burugupally:** Funding acquisition, Project administration, Resources, Writing - review & editing. **Ethan McDaniel:** Writing - review & editing. **Jared D. Hobeck:** Funding acquisition, Project administration, Writing - review & editing.

Declaration of Competing Interest

The authors declare that they have no known competing financial interests or personal relationships that could have appeared to influence the work reported in this paper.

Acknowledgments

This material is based upon work supported by the National Aeronautics and Space Administration under Grant No. 80NSSC19M0042. Any opinions, findings, and conclusions or recommendations expressed in this material are those of the author(s) and do not necessarily reflect the views of any or all of the following: National Aeronautics and Space Administration, the Wichita State University, the University of Kansas, and Kansas State University.

References

[1] Ghojel JI. Review of the Development and Applications of the Wiebe Function: A Tribute to the Contribution of Ivan Wiebe to Engine Research. Int J Engine Res 2010;11(4):297–312. https://doi.org/10.1243/14680874jer06510.

[2] Bade M, Clark NN, Robinson MC, Famouri P. Parametric Investigation of Combustion and Heat Transfer Characteristics of Oscillating Linear Engine Alternator. J Combust 2018;2018:1–16. https://doi.org/10.1155/2018/2907572.

[3] Bade RMB. Measured and Modeled Performance of a Spring Dominant Free Piston Engine Generator. Ph.D. Dissertation. In: Mechanical and Aerospace Engineering. West Virginia University; 2020. https://doi.org/10.33915/etd.7528.

[4] Robinson MC, Clark NN. Study on the Use of Springs in a Dual Free Piston Engine Alternator. International Powertrains, Fuels & Lubricants Meeting (2016). SAE International. (Paper Number: 2016-01-2233. doi: 10.4271/2016-01-2233.

[5] Heywood JB. Internal Combustion Engine Fundamentals. 2nd ed. New York: McGraw-Hill Education; 2018. ISBN: 9781260116106.

[6] Navarro E, Leo TJ, Corral R. CO_2 Emissions from a Spark Ignition Engine Operating on Natural Gas-Hydrogen Blends (HCNG). Appl Energy 2013;101:112–20. https://doi.org/10.1016/j.apenergy.2012.02.046.

[7] Johansson T, Borgqvist P, Johansson B, Tunestal P, Aulin H. HCCI Heat Release Data for Combustion Simulation, Based on Results from a Turbocharged Multi-cylinder Engine. International Powertrains, Fuels & Lubricants Meeting (2010). SAE International. (Paper Number: 2010-01-1490). doi: 10.4271/2010-01-1490.

[8] Kim J, Bae C, Kim G. Simulation on the Effect of the Combustion Parameters on the Piston Dynamics and Engine Performance Using the Wiebe Function in a Free Piston Engine. Appl Energy 2013;107:446–55. https://doi.org/10.1016/j.apenergy.2013.02.056.

[9] Kumar R, Reader GT, Zheng M. A Preliminary Study of Ignition Consistency and Heat Release Analysis for a Common-Rail Diesel Engine. World Congress & Exhibition (2004). SAE International. (Paper Number: 2004-01-0932). doi: 10.4271/2004-01-0932.

[10] Rahman MMK, Hamada I, Noor MM, Rosli AB, Kadirgama K, Maleque MA. In-Cylinder Heat Transfer Characteristics Of Hydrogen Fueled Engine: A Steady State Approach. Am J Environ Sci 2010;6(2):124–9. https://doi.org/10.3844/ajessp.2010.124.129.

[11] Ravaglioli V, Moro D, Serra G, Ponti F. MFB50 On-Board Evaluation Based On A Zero-Dimensional ROHR Model. World Congress & Exhibition (2011). SAE International. (Paper Number: 2011-01-1420). doi: 10.4271/2011-01-1420.

[12] Rousseau S, Lemoult B, Tazerout M. Combustion Characterization of Natural Gas in a Lean Burn Spark-Ignition Engine. Proc Inst Mech Eng Part D: J Autom Eng 1999;213(5):481–9. https://doi.org/10.1243/0954407991527044.

[13] Watts PA, Heywood JB. Simulation Studies of the Effects of Turbocharging and Reduced Heat Transfer on Spark-ignition Engine Operation. Automotive Engineering Congress and Exposition (1980). SAE International. (Paper Number: 800289). doi: 10.4271/800289.

[14] Yeliana Y, Cooney C, Worm J, Michalek DJ, Naber JD. Estimation of Double-Wiebe Function Parameters Using Least Square Method for Burn Durations of Ethanol-Gasoline Blends in Spark Ignition Engine over Variable Compression Ratios and EGR Levels. Appl Therm Eng 2011;31(14–15):2213–20. https://doi.org/10.1016/j.applthermaleng.2011.01.040.

[15] Melaika M, Andersson M, Dahlander P. Methane Direct Injection in an Optical SI Engine - Comparison between Different Combustion Modes. International Powertrains, Fuels & Lubricants Meeting (2019). SAE International. (Paper Number: 2019-01-0083). doi: 10.4271/2019-01-0083.

[16] Langness C, Mattson J, Depcik C. Moderate Substitution of Varying Compressed Natural Gas Constituents for Assisted Diesel Combustion. Combust Sci Technol 2017;189(8):1354–72. https://doi.org/10.1080/00102202.2017.1295040.

[17] Ash RL, Dowler WL, Varsi G. Feasibility of Rocket Propellant Production on Mars. Acta Astronaut 1978;5(9):705–24. https://doi.org/10.1016/0094-5765(78)90049-8.

[18] Trinh H. Liquid Methane/Oxygen Injector Study for Potential Future Mars Ascent. 36th AIAA/ASME/SAE/ASEE Joint Propulsion Conference and Exhibit (2000). American Institute of Aeronautics and Astronautics. doi: 10.2514/6.2000-3119.

[19] OWEN TOBIAS. In: Mars. University of Arizona Press; 2018. p. 818–34. https://doi.org/10.2307/j.ctt207g59v.29.

[20] European Space Agency. ESA - Robotic Exploration of Mars - Comparing the Atmospheres of Mars and Earth; 2018. Available from: https://exploration.esa.int/web/mars/-/60153-comparing-the-atmospheres-of-mars-and-earth. 2020].

[21] Hoffman SJ, Kaplan DI. Human Exploration of Mars: The Reference Mission of the NASA Mars Exploration Study Team. CreateSpace Independent Publishing Platform; 1997.

[22] Terraforming FMJ. Engineering Planetary Environments. SAE International; 1995.

[23] Palaszewski BA. Atmospheric Mining in the Outer Solar System: Aerial Vehicle Reconnaissance and Exploration Options. In: 50th AIAA/ASME/SAE/ASEE Joint Propulsion Conference; 2014. https://doi.org/10.2514/6.2014-3819.

[24] Palaszewski BA. Atmospheric Mining in the Outer Solar System: Resource Capturing, Exploration, and Exploitation. In: 49th AIAA/ASME/SAE/ASEE Joint Propulsion Conference; 2013. https://doi.org/10.2514/6.2013-3765.

[25] Fraser S, Monsberger M, Hacker V. Fuel Cell Power System Options for Mars Rovers. 557. European Space Agency Special. Publication 2004:15.1..

[26] Fraser SD. Fuel Cell Power System Options for Mars Surface Mission Elements. In: Badescu V, editor. Mars: Prospective Energy and Material Resources. Berlin Heidelberg: Springer Berlin Heidelberg; 2009. p. 139–74.

[27] Vilekar S, Junaedi C, Gao Z, Howard C, Roychoudhury S. Regenerative Solid Oxide Stack for Lunar and Mars Oxygen Production and Surface Energy Storage. 48th International Conference on Environmental Systems. 2018.

[28] Depcik C, Cassady T, Collicott B, Burugupally SP, Li X, Alam SS, et al. Comparison of Lithium Ion Batteries, Hydrogen Fueled Combustion Engines, and a Hydrogen Fuel Cell in Powering a Small Unmanned Aerial Vehicle. Energy Convers Manage 2020;207. https://doi.org/10.1016/j.enconman.2020.112514.

[29] Bui H, Coletta C, Debois A. Mars Methane Engine. National Aeronautics and Space Administration, NASA-CR-197205; 1994.
[30] Colozza AJ. Comparison of Mars Aircraft Propulsion Systems; 2003.
[31] Zubrin R, Baker D, Gwynne O. Mars Direct - A Simple, Robust, and Cost Effective Architecture for the Space Exploration Initiative. In: 29th Aerospace Sciences Meeting; 1991. https://doi.org/10.2514/6.1991-329.
[32] Thurnheer T, Soltic P, Eggenschwiler PDSI. Engine Fuelled with Gasoline, Methane and Methane/Hydrogen Blends: Heat Release and Loss Analysis. Int J Hydrogen Energy 2009;34(5):2494–503. https://doi.org/10.1016/j.ijhydene.2008.12.048.
[33] Seboldt D, Lejsek D, Bargende M. Injection Strategies for Low HC Raw Emissions in SI Engines with CNG Direct Injection. Automotive Engine Technol 2016;1(1–4): 81–91. https://doi.org/10.1007/s41104-016-0002-4.
[34] Mokhatab S, Poe WA, Mak JY. Natural Gas Fundamentals. Handbook Nat Gas Transmiss Process 2019:1–35.
[35] Diaz GJA, Montoya JPG, Martinez LAC, Olsen DB, Navarro AS. Influence of Engine Operating Conditions on Combustion Parameters in a Spark Ignited Internal Combustion Engine Fueled with Blends of Methane and Hydrogen. Energy Convers Manage 2019;181:414–24. https://doi.org/10.1016/j.enconman.2018.12.026.
[36] Amador German, Yepes Hernando A, Gonzalez-Quiroga Arturo, Bula Antonio. Development of Extended Formulations of the Relative Concentration of Chain Carrier Method for Knock Prediction in Spark-Ignited Internal Combustion Engines Fueled with Gaseous Fuels. Fuel 2020;279:118352. https://doi.org/10.1016/j.fuel.2020.118352.
[37] Asgari O, Hannani SK, Ebrahimi R. Improvement and Experimental Validation of a Multi-Zone Model for Combustion and NO Emissions in CNG Fueled Spark Ignition Engine. J Mech Sci Technol 2012;26(4):1205–12. https://doi.org/10.1007/s12206-012-0229-6.
[38] Cordeiro De Melo TC, Machado GB, Machado RT, Pereira Belchior CR, Pereira PP. Thermodynamic Modeling of Compression, Combustion and Expansion Processes of Gasoline, Ethanol and Natural Gas with Experimental Validation on a Flexible Fuel Engine. 8th International Conference on Engines for Automobiles (2007). Consiglio Nazionale delle Ricerche. (Paper Number: 2007-24-0035). doi: 10.4271/2007-24-0035.
[39] Dudgeon RJ. An Exergy-Based Analysis of Gasification and Oxyburn Processes. In: Mechanical Engineering. MS: The University of Iowa; 2009. p. 114. https://doi.org/10.17077/etd.788qfnzb.
[40] Ghazal OH. A Comparative Evaluation of the Performance of Different Fuel Induction Techniques for Blends Hydrogen-Methane SI Engine. Int J Hydrogen Energy 2013;38(16):6848–56. https://doi.org/10.1016/j.ijhydene.2013.03.090.
[41] Przybyła G, Postrzednik S, Żmudka Z. Correlations of Wiebe Function Parameters for Combustion Simulation in SI Engine Fuelled with Gaseous Fuels. J KONES Powertrain Transp 2016;23(2):293–300. https://doi.org/10.5604/12314005.1213724.
[42] Yıldız M, Çeper BA. Zero-Dimensional Single Zone Engine Modeling of an Si Engine Fuelled with Methane and Methane-Hydrogen Blend Using Single and Double Wiebe Function: A Comparative Study. Int J Hydrogen Energy 2017;42(40): 25756–65. https://doi.org/10.1016/j.ijhydene.2017.07.016.
[43] Nguyen Duc-Khanh, Szybist James, Sileghem Louis, Verhelst Sebastian. Effects of Molar Expansion Ratio of Fuels on Engine Efficiency. Fuel 2020;263:116743. https://doi.org/10.1016/j.fuel.2019.116743.
[44] Liu J, Dumitrescu CE. Single and Double Wiebe Function Combustion Model for a Heavy-Duty Diesel Engine Retrofitted to Natural-Gas Spark-Ignition. Appl Energy 2019;248:95–103. https://doi.org/10.1016/j.apenergy.2019.04.098.
[45] Samanta A, Das S, Roy PC. Performance Analysis of a Biogas Engine. Int J Res Eng Technol 2016;05(13):67–71. https://doi.org/10.15623/ijret.2016.0513012.
[46] Shudo T, Nabetani S. Analysis of Degree of Constant Volume and Cooling Loss in a Hydrogen Fuelled SI Engine. SAE International Fall Fuels & Lubricants Meeting & Exhibition (2001). SAE International. (Paper Number: 2001-01-3561), https://doi.org/10.4271/2001-01-3561.
[47] Toman R, Polóni M, Chríbik A. Preliminary Study on Combustion and Overall Parameters of Syngas Fuel Mixtures for Spark Ignition Combustion Engine. Acta Polytechnica 2017;57(1):38–48. https://doi.org/10.14311/AP.2017.57.0038.
[48] Zhou Y, Sofianopoulos A, Gainey B, Lawler B, Mamalis S. A System-Level Numerical Study of a Homogeneous Charge Compression Ignition Spring-Assisted Free Piston Linear Alternator with Various Piston Motion Profiles. Appl Energy 2019;239:820–35. https://doi.org/10.1016/j.apenergy.2019.01.240.
[49] Alam SS, Depcik C. Adaptive Wiebe Function Parameters for a Port-Fuel Injected Hydrogen-Fueled Engine. Volume 8: Heat Transfer and Thermal Engineering (2019). American Society of Mechanical Engineers. doi: 10.1115/imece2019-10031.
[50] Rahman MMK, Mohammed MK, Bakar RA. Effects of Air-Fuel Ratio and Engine Speed on Performance of Hydrogen Fueled Port Injection Engine. J Appl Sci 2009;9(6):1128–34. https://doi.org/10.3923/jas.2009.1128.1134.
[51] Piehl JA, Zyada A, Bravo L, Samimi-Abianeh O. Review of Oxidation of Gasoline Surrogates and Its Components. J Combust 2018;2018:1–27. https://doi.org/10.1155/2018/8406754.
[52] Olalekan SW, Aziz RA, Dahlan A. Combustion Characteristics of Spark Ignition Engine Fuelled by Compressed Natural Gas in a Direct Injection Compressed Natural Gas Engine. Int J Appl Eng Res 2018;13(1):727–31.
[53] Babu MS, Garg V, Akella SB, Clement S, Rajan NKS. Influence of Valve Lift Timing on Producer Gas Combustion and Its Modeling Using Two-Stage Wiebe Function. 2017. doi: 10.5281/zenodo.1129636.
[54] Gutierrez RHR. Comportamiento Termodinamico De Un Grupo Diesel Generador Convertido Para Uso Exclusivo De Gas Natural. Facultad De Ingenieria Mecanica. M.S. Lima-Peru: Universidad Nacional De Ingenieria; 2012.
[55] Hagos FY, Abd Aziz AR. Mass Fraction Burn Investigation of Lean Burn Low BTU Gasification Gas in Direct-Injection Spark-Ignition Engine. World Congress & Exhibition (2014). SAE International. (Paper Number: 2014-01-1336). doi: 10.4271/2014-01-1336.
[56] Liu J, Dumitrescu CE. Improved Thermodynamic Model for Lean Natural Gas Spark Ignition in a Diesel Engine Using a Triple Wiebe Function. J Energy Res Technol 2020;142(6). https://doi.org/10.1115/1.4045534.
[57] Rohatgi A. WebPlotDigitizer, Version: 3.8, 2020, Available from: https://automeris.io/WebPlotDigitizer.
[58] Sandhu SS, Babu MKG, Das LM. Investigations of Emission Characteristics and Thermal Efficiency in a Spark-Ignition Engine Fuelled with Natural Gas-Hydrogen Blends. Int J Low-Carbon Technol 2011;8(1):7–13. https://doi.org/10.1093/ijlct/ctr038.
[59] Tabaczynski R, Trinker F, Shannon B. Further Refinement and Validation of a Turbulent Flame Propagation Model for Spark-Ingition Engines. Combust Flame 1980;39(2):111–21. https://doi.org/10.1016/0010-2180(80)90011-5.
[60] Briutov AA, Senachin AP, Senachin PK. Turbulent Charge Burning in SI Engines. J Phys: Conf Ser 2019:1382. https://doi.org/10.1088/1742-6596/1382/1/012065.
[61] Poetsch C, Wurzenberger J, Katrasnik T. A Real-Time Capable and Modular Modeling Concept for Virtual SI Engine Development. WCX SAE World Congress Experience (2020). SAE International. (Paper Number: 2020-01-0577). doi: 10.4271/2020-01-0577.
[62] Benim AC, Syed KJ. Concepts Related to Combustion and Flow in Premix Burners. In: Flashback Mechanisms in Lean Premixed Gas Turbine Combustion; 2015. p. 5–18.
[63] Sakhrieh A. The Adiabatic Flame Temperature and Laminar Flame Speed of Methane Premixed Flames at Varying Pressures. Acta Periodica Technologica 2019;50:220–7. https://doi.org/10.2298/apt1950220s.
[64] Varghese RJ, Kolekar H, Kishore VR, Kumar S. Measurement of Laminar Burning Velocities of Methane-Air Mixtures Simultaneously at Elevated Pressures and Elevated Temperatures. Fuel 2019;257:116120. https://doi.org/10.1016/j.fuel.2019.116120.
[65] Akram M, Saxena P, Kumar S. Laminar Burning Velocity of Methane-Air Mixtures at Elevated Temperatures. Energy Fuels 2013;27(6):3460–6. https://doi.org/10.1021/ef4009218.
[66] Pizzuti L, Martins CA, dos Santos LR, Guerra DRS. Laminar Burning Velocity of Methane/Air Mixtures and Flame Propagation Speed Close to the Chamber Wall. Energy Procedia 2017;120:126–33. https://doi.org/10.1016/j.egypro.2017.07.145.
[67] Baigmohammadi M, Tabejamaat S, Yeganeh M. Experimental Study of Methane-Oxygen Premixed Flame Characteristics in Non-Adiabatic Micro-Reactors. Chem. Eng. Process. – Process Intensif. 2019;142:107590. https://doi.org/10.1016/j.cep.2019.107590.
[68] McNesby KL, Daniel RG, Miziolek AW, Babushok VI, Cheskis S. Flame Velocimetry Measurements of Inhibited Methane/Oxygen Flames Using Pulsed Flame Velocimetry. Army Research Lab Aberdeen Proving Ground MD; 1995.
[69] Oh J, Noh D. Laminar Burning Velocity of Oxy-Methane Flames in Atmospheric Condition. Energy 2012;45(1):669–75. https://doi.org/10.1016/j.energy.2012.07.027.
[70] Dyakov IV, Konnov AA, Ruyck JD, Bosschaart KJ, Brock ECM, De Goey LPH. Measurement of Adiabatic Burning Velocity in Methane-Oxygen-Nitrogen Mixtures. Combust Sci Technol 2001;172(1):81–96. https://doi.org/10.1080/00102200108935839.
[71] Mazas AN, Fiorina B, Lacoste DA, Schuller T. Effects of Water Vapor Addition on the Laminar Burning Velocity of Oxygen-Enriched Methane Flames. Combust Flame 2011;158(12):2428–40. https://doi.org/10.1016/j.combustflame.2011.05.014.
[72] Der Damköhler G. Einfluss der Turbulenz auf die Flammengeschwindigkeit in Gasgemischen. Zeitschrift für Elektrochemie und angewandte physikalische Chemie 1940;46(11):601–26. https://doi.org/10.1002/bbpc.19400461102.
[73] Ratzke A, Schöffler T, Kuppa K, Dinkelacker F. Validation of Turbulent Flame Speed Models for Methane-Air Mixtures at High Pressure Gas Engine Conditions. Combust Flame 2015;162(7):2778–87. https://doi.org/10.1016/j.combustflame.2015.04.011.
[74] Kobayashi H. Experimental Study of High-Pressure Turbulent Premixed Flames. Exp Therm Fluid Sci 2002;26(2–4):375–87. https://doi.org/10.1016/S0894-1777(02)00149-8.
[75] Kang Z, Wu Z, Zhang Z, Deng J, Hu Z, Li L. Study of the Combustion Characteristics of a HCCI Engine Coupled with Oxy-Fuel Combustion Mode. SAE Int J Engines 2017;10(3):908–16. https://doi.org/10.4271/2017-01-0649.
[76] Van Blarigan A, Kozarac D, Seiser R, Cattolica R, Chen J-Y, Dibble R. Experimental Study of Methane Fuel Oxycombustion in a Spark-Ignited Engine. J Energy Res Technol 2014;136(1). https://doi.org/10.1115/1.4024974.